A High Gain Grid Connected Single Stage Inverter System with Reactive Power Control

T. Sreekanth
Student Member, IEEE
Department of Electrical Engineering
Indian Institute of Technology Madras
Chennai, India-600036.

N. Lakshmi Narasamma
Member, IEEE
Department of Electrical Engineering
Indian Institute of Technology Madras
Chennai, India-600036.

Mahesh K. Mishra
Senior Member, IEEE
Department of Electrical Engineering
Indian Institute of Technology Madras
Chennai, India-600036.

***Abstract*—Single stage converter system (SSCS) does both dc-dc conversion and dc-ac conversion in one stage. In this paper, a SSCS for photovoltaic (PV) applications is presented. This system can deliver active power from PV to the grid while continuously tracking maximum power point (MPP). The proposed system is controlled such that it can deliver/receive reactive power from grid. The presented system has several advantages like high gain, low switching loss and compact in size. This system can be used effectively in PV systems, where output voltage of PV is very low. Control scheme of the system along with derivation of control loops is presented. The proposed topology is simulated using MATLAB/SIMULINK, simulation results are presented to validate the proposed idea.**

Index Terms: Single stage, high gain, MPP, photovoltaic, buck-boost inverter.

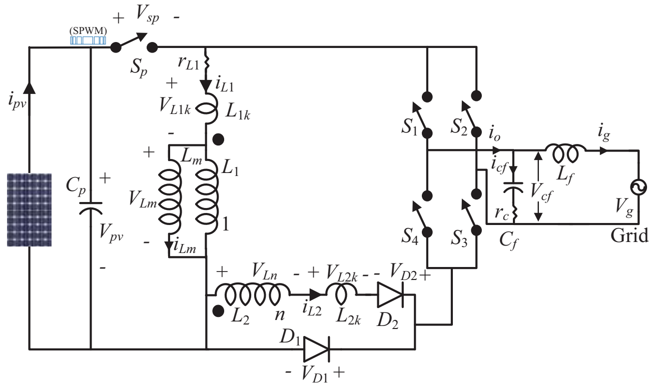

Fig. 1. Grid connected single-stage PV system configuration

I. Introduction

Output voltage of PV varies with insolation, temperature etc. So, a suitable power conversion system (PCS) is essential in order to deliver power from PV to loads or grid. Especially, for delivering power to grid, PCS has to step up/down the output voltage from PV and then convert it into ac. This is a two stage conversion system (TSCS). Many two stage PCS are mentioned in [1]. TSCS posses several disadvantages like less reliability, more losses, bulk in size and high cost [2]. So, a PCS which can efficiently buck/boost the output voltage from PV and perform dc-ac power conversion simultaneously with maximum power point tracking (MPPT) is required in this scenario. Single stage converter system (SSCS) which does both dc-dc conversion and dc-ac conversion in a single stage is well suitable. SSCS is reliable, operates at higher efficiencies and less costly [3].

Jain et al. proposed a buck-boost principle based topology in [4], which has several advantages like less number of switches, low switching loss and less EMI problems. The main drawback of this topology is limited gain. Patel et al., proposed a SSCS which is doubly grounded in [5]. This scheme has less number of components and more compact, but it gives low gain. Reactive power control operation is not presented in [4], [5]. Some high gain SSCS schemes are presented in [6], [7]. In these schemes, coupled inductor is used in order to get high gain. These schemes suffers from harmful effects due to leakage inductance associated with coupled inductor. Hence, these schemes are suitable for low power applications only. A single stage three phase grid connected photovoltaic system with modified MPPT method and reactive power compensation is presented in [8]. This control method is based on instantaneous reactive power theory. This method consists of more calculations as it involves transformations. This control method is a good choice for reactive power control in three phase systems and the proposed system in this work is suitable for low voltage gain conditions only. Hosseini et al. proposed a single phase series grid connected PV system for voltage compensation and for power supply in [9]. This system consists of a boost inverter that supplies a household load in different operating conditions such as grid connection and islanding. As this system works with buck-boost principle, the switching losses are more and achievable voltage gain is limited.

Reactive power control schemes along with maximum power point tracking are presented in [10], [11]. Though these schemes works effectively in low voltage gain conditions, the performance of these schemes degrade at high voltage gain conditions. The single stage inverter system presented in [12] has several advantages like less number of components, high gain and does not need additional capacitors to trap leakage energy. So, this system along with reactive power control scheme is presented in this paper. A brief comparison of presented system with existed systems is presented in Table I. In this paper, a high gain single stage inverter system along with reactive power control is presented. The remaining of this paper is organized as follows. Introduction of grid connected SSCS is presented in Section II. Section III gives MPPT along with the control scheme for the converter. Simulation studies are presented in Section IV, followed by conclusion in Section V.

II. Grid connected single-stage PV system

Presented PV fed SSCS consists of five active switches $(S_p, S_1, S_2, S_3, S_4)$, two passive switches $(D_1$ & $D_2)$, a coupled inductor $(L_1$ & $L_2)$, output side filter circuit $(C_f$ & $L_f)$ and an input side filter capacitor (C_p) as shown in Fig. 1. During each half cycle of output voltage, switch (S_p) operates at high frequency, where as switches (S_1, S_3) and switches (S_2, S_4) are switched on continuously for entire alternative half cycle of output voltage. In every switching cycle, during S_p on time, v_{pv} charges L_1, where as during S_p off time, inductors $(L_1$ & $L_2)$ come in series and discharge into output capacitor (C_f). Diode (D_1) is used to remove the harmful effects of leakage inductance of the coupled inductor. This SSCS has features like high voltage gain, low switching loss and compact in size. The voltage gain of the topology $(g(t))$ is given by

$$g(t) = \frac{v_{cf}(t)}{v_{pv}} = \frac{(1+n)d(t)}{1-d(t).} \tag{1}$$

Where 'n' is turns ratio of the coupled inductor and 'd' is duty cycle of the switch (S_p). The design value of capacitor (C_p) is given by [4]

$$C_p = \frac{2P}{4(2\pi f_g)\ V_{pv}\ \delta V_{pv}} \tag{2}$$

where 'P' is the maximum power to be tracked, δV_{pv} be the maximum value of the permissible ripple in the PV voltage and f_g be the grid voltage fundamental frequency. A brief introduction of the single stage inverter topology for different loads along with details like gain derivation, analytical waveforms and voltage stresses across the switches are presented in [12].

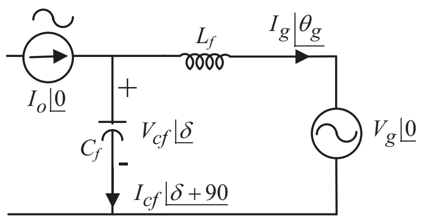

Fig. 2. Output circuit of SSCS.

III. Maximum Power Point Tracking and Reactive Power Control Technique

MPPT is to automatically tracking the voltage or current at which a PV array should operate in order to obtain the maximum power output for a given irradiation and temperature. In this paper "Perturb and Observe Method" [13] is used to track the maximum power point (MPP) of the PV source. This

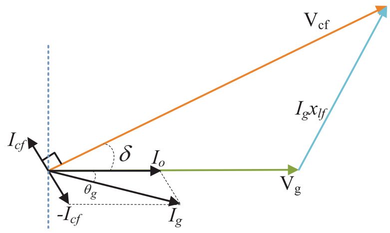

Fig. 3. Phasor diagram related to output circuit.

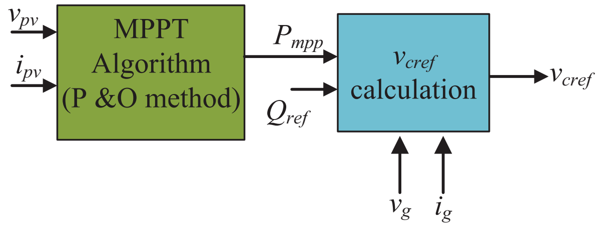

Fig. 4. Reference voltage generation for output capacitor (C_f).

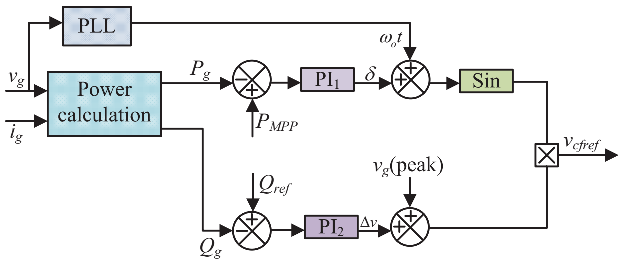

Fig. 5. Block diagram for V_{cfref} calculation.

algorithm has been appropriately implemented in conjunction with the grid connected presented system to deliver maximum power to grid. After finding the current i_{MPP}, if this current is multiplied with grid template [4], [5] and is given to track in L_1 using current controller i.e.. output current (i_o) which is in phase with grid voltage will appear before filtering circuit $(C_f$ & $L_f)$ as shown in Fig. 2. Because of the filtering circuit, a phase shift will be added to i_o making grid current not in phase with the grid voltage. This phase shift can be observed from phasor diagram of output circuit shown in Fig. 3. So, in order to control this phase difference between grid voltage and grid current to have variable reactive power flow, following control scheme is implemented. At first we calculate P_{MPP} using P & O method, then this P_{MPP} and reference reactive power (Q_{ref}) are used to calculate output capacitor voltage (v_{cf}) which is required to send both MPP power and reference reactive power to grid as shown in Fig. 4. Block diagram for calculation of v_{cfref} is shown in Fig. 5. After finding voltage (v_{cf}), reference current generation (i_{L1mref}) will be done using voltage control loop as shown in Fig. 7. Finally, the generated reference current (i_{Lmref}) will be tracked using current control loop as shown in Fig. 8. Pulses to all active switches are generated as shown in Fig. 9. In this

TABLE I
A BRIEF COMPARISON OF PROPOSED GCSS WITH THE EXISTING GCSS

	Source	Control variable	P_g	Q_g	Remarks
Jain [4]	PV	Current	MPP	Un controllable	Low gain and less loss.
Patel [5]	PV	Current	MPP	Un controllable	Low gain and more conduction loss.
Libo [8]	PV	Current	MPP	Controllable	Low voltage gain.
Hosseini [9]	PV	Voltage	MPP	Controllable	Low voltage gain and more switching loss.
Jang [10]	FC	Voltage	Controllable	Controllable	Low gain, more loss, EMI problems and PR control.
Alajmi [11]	PV	Current	MPP	Controllable	More components and complex control.
Proposed	PV	Voltage	MPP	Controllable	High gain, less loss and PI control.

way, reactive power is controlled while delivering MPP power to the grid.

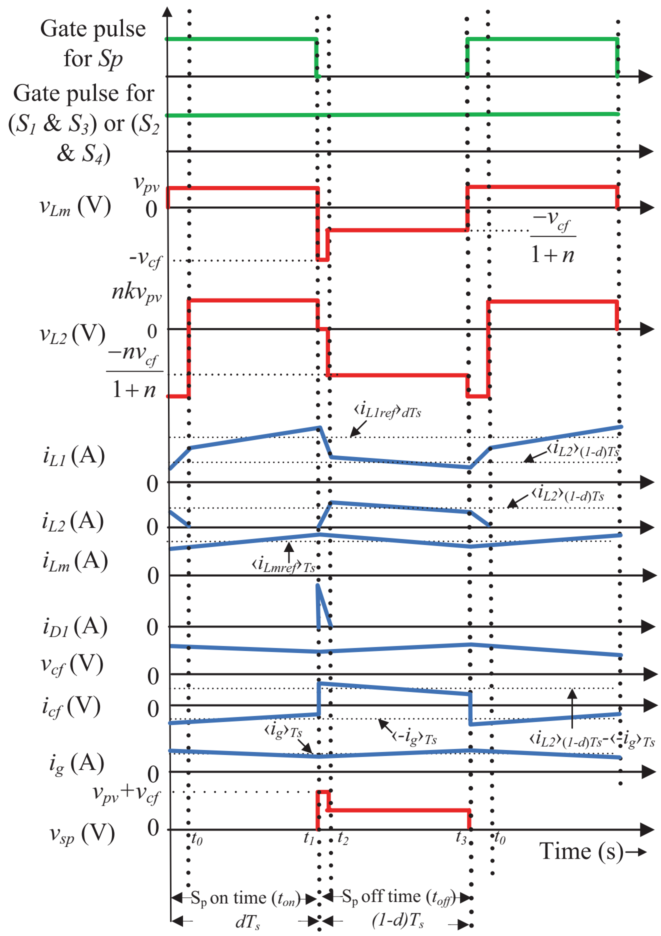

Fig. 6. GCSS operation over a switching cycle.

A. Design of Voltage Controller

Voltage control loop is derived by using average current through capacitor (C_f) over a switching cycle. From Fig. 6, during switch (S_p) on time (dT_s) current through capacitor (C_f) equals to $-i_g$ and during switch (S_p) off time ((1-$d)T_s$), the current through capacitor (C_f) is $(\langle i_{L2}(t)\rangle_{(1-d)Ts} - \langle i_g(t)\rangle_{Ts})$. Assuming negligible leakage inductance and negligible current ripple in inductors, current through capacitor (C_f) over a switching cycle is given by

$$\langle i_{cf}(t)\rangle_{Ts} = (1-d(t))\langle i_{L2}(t)\rangle_{(1-d)Ts} - \langle i_g(t)\rangle_{Ts}. \quad (3)$$

Where $\langle i_{cf}(t)\rangle_{Ts}$, $\langle i_g(t)\rangle_{Ts}$ and $\langle i_{L2}(t)\rangle_{(1-d)Ts}$ are average current through C_f, average current sending to grid over a switching cycle (T_s) and average current in L_2 over $(1-d(t)Ts)$. From (3), $\langle i_{L2}(t)\rangle_{(1-d)Ts}$ can be written as

$$\langle i_{L2}(t)\rangle_{(1-d)Ts} = \frac{\langle i_{cf}(t)\rangle_{Ts} + \langle i_g(t)\rangle_{Ts}}{1-d(t)}. \quad (4)$$

From [12], gain of converter is given by

$$\frac{\langle v_{cf}(t)\rangle_{Ts}}{\langle v_{pv}(t)\rangle_{Ts}} = \frac{(1+n)d(t)}{1-d(t)}. \quad (5)$$

From the above equation $1/(1-d(t))$ can be written as

$$\frac{1}{1-d(t)} = \frac{\langle v_{cf}(t)\rangle_{Ts} + \langle v_{pv}(t)\rangle_{Ts}(1+n)}{\langle v_{pv}(t)\rangle_{Ts}(1+n)}. \quad (6)$$

Substituting (6) in (4) gives

$$\langle i_{L2}(t)\rangle_{(1-d)Ts} = \\ (\langle i_{cf}(t)\rangle_{Ts} + \langle i_g(t)\rangle_{Ts})\{\frac{\langle v_{cf}(t)\rangle_{Ts} + \langle v_{pv}(t)\rangle_{Ts}(1+n)}{\langle v_{pv}(t)\rangle_{Ts}(1+n)}\}. \quad (7)$$

From [12], $\langle i_{L1ref}(t)\rangle_{dTs}$ can be written as

$$\langle i_{L1ref}(t)\rangle_{dTs} = (1+n)\ \langle i_{L2}(t)\rangle_{(1-d)Ts} \quad (8)$$

From (7) and (8), i_{L1ref} can be written as

$$\langle i_{L1ref}(t)\rangle_{dTs} = \\ (\langle i_{cf}(t)\rangle_{Ts} + \langle i_g(t)\rangle_{Ts})\{\frac{\langle v_{cf}(t)\rangle_{Ts} + \langle v_{pv}(t)\rangle_{Ts}(1+n)}{\langle v_{pv}(t)\rangle_{Ts}}\}. \quad (9)$$

From the operation of GCSS, i_{L1ref} is equal to i_{Lmref} during switch (S_p) on time. Therefore

$$\langle i_{Lmref}(t)\rangle_{dTs} = A = \\ (\langle i_{cf}(t)\rangle_{Ts} + \langle i_g(t)\rangle_{Ts})\{\frac{\langle v_{cf}(t)\rangle_{Ts} + \langle v_{pv}(t)\rangle_{Ts}(1+n)}{\langle v_{pv}(t)\rangle_{Ts}}\}. \quad (10)$$

Here, 'A' is used to represent a block in Fig. 7. Double-loop control presented in [14] is used for controlling both v_{cf} and i_{Lm}. By taking $\langle i_{cf}\rangle_{Ts}$ as control variable, voltage control block diagram of the topology can be written as shown in Fig. 7. Here r_c is the equivalent series resistance associated with C_f and $v_{cfref}(t)$ is calculated based on the available nominal PV power.

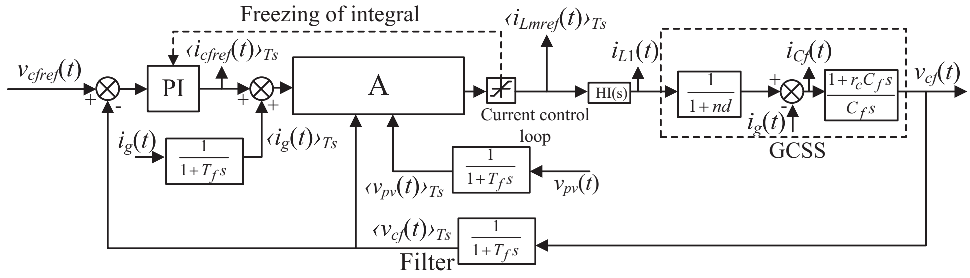

Fig. 7. Control loop for v_{cref} tracking.

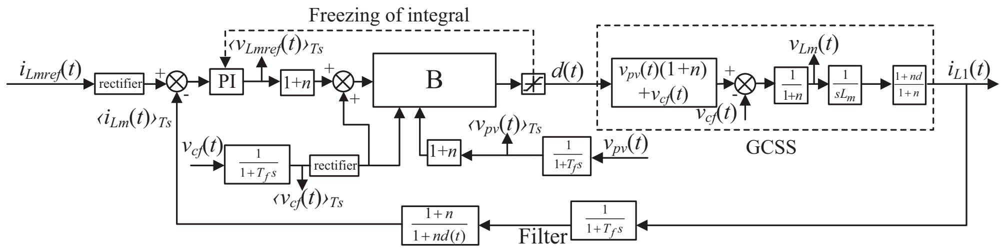

Fig. 8. Block diagram for mutual inductance current (i_{Lm}) control (current control loop (HI(s))).

B. Design of Current Controller

To design current controller, the operation of the proposed converter over a switching cycle is considered as shown in Fig. 6. From Fig. 6, during switch (S_p) on time (dT_s) voltage across L_m is input voltage (v_{pv}) and during switch (S_p) off time ($(1-d)T_s$) the voltage across L_m is $-v_{cf}/(1+n)$. Average voltage across L_m over switching cycle is given by

$$\langle v_{Lm}\rangle_{Ts} = \langle v_{pv}\rangle_{Ts} d(t) - \frac{(1-d(t))\langle v_{cf}(t)\rangle_{Ts}}{1+n}. \tag{11}$$

From above equation '$d(t)$' can be written as

$$d(t) = \frac{\langle v_{Lm}(t)\rangle_{Ts}(1+n) + \langle v_{cf}(t)\rangle_{Ts}}{\langle v_{pv}(t)\rangle_{Ts}(1+n) + \langle v_{cf}(t)\rangle_{Ts}} = B. \tag{12}$$

Here, 'B' is used to represent a block in Fig. 8. From Fig. 6, calculation of i_{Lm} over a switching cycle is shown below.

$$\begin{aligned}\langle i_{L1}(t)\rangle_{Ts} =& \langle i_{L1ref}(t)\rangle_{dTs} d(t) + \langle i_{L2}(t)\rangle_{(1-d)Ts}(1-d(t))\\ =& \langle i_{Lmref}(t)\rangle_{dTs} d(t) + \frac{\langle i_{Lmref}(t)\rangle_{dTs}}{1+n}(1-d(t))\\ =& \langle i_{Lmref}(t)\rangle_{Ts}\frac{(1+nd(t))}{1+n}.\end{aligned} \tag{13}$$

Where $\langle i_{L1}(t)\rangle_{Ts}$ is the average of i_{L1} over a switching cycle (T_s). From eqn (13), $\langle i_{Lm}(t)\rangle_{Ts}$ can be written as

$$\langle i_{Lm}(t)\rangle_{Ts} = \langle i_{L1}(t)\rangle_{Ts}\frac{(1+n)}{1+nd(t)}. \tag{14}$$

By taking $\langle v_{Lm}\rangle_{Ts}$ as control variable, using control method in [14], current control loop block diagram of the topology can be written as shown in Fig. 8. The gains of the PI controllers are chosen such that the current loop has a bandwidth of 4 kHz and 60° phase margin and voltage control loop has a bandwidth of 4 kHz and 60° phase margin. Gating pulses for all active switches are generated as shown in Fig. 9.

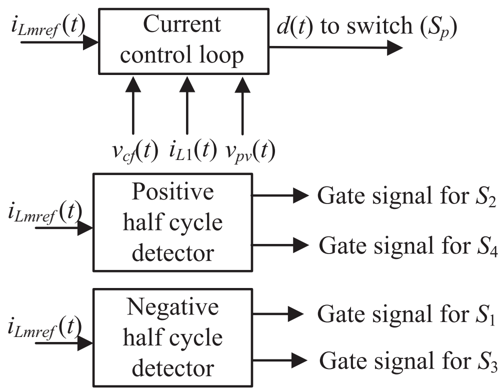

Fig. 9. Block diagram of pulses generation for active switches.

IV. Simulation Studies

Presented grid connected SSCS is simulated using MATLAB/SIMULINK with the parameters mentioned in Table II. The system is tested under different irradiation levels (1000W/m^2, 450W/m^2 and 750W/m^2) and different temperature (313 K, 295 K and 305 K) conditions for Unity Power Factor operation (UPF) at $t = 0$s, $t = 1$s and $t = 2$s shown in Fig. 10. The corresponding results are shown in Fig. 10, Fig. 11 and Fig. 12. Different tested insolation and temperature conditions are shown in Fig. 10(a), and Fig. 10(b). Obtained PV side results PV power, PV voltage and PV current are shown in Fig. 10(c), Fig. 10(d), and Fig. 10(e) respectively. From Fig. 10(c) it is observed that at each condition, the system is tracking MPP with minimum ripple in the PV power. The dotted areas in Fig. 10(c) indicate the MPP regions at which system is operating at each insolation

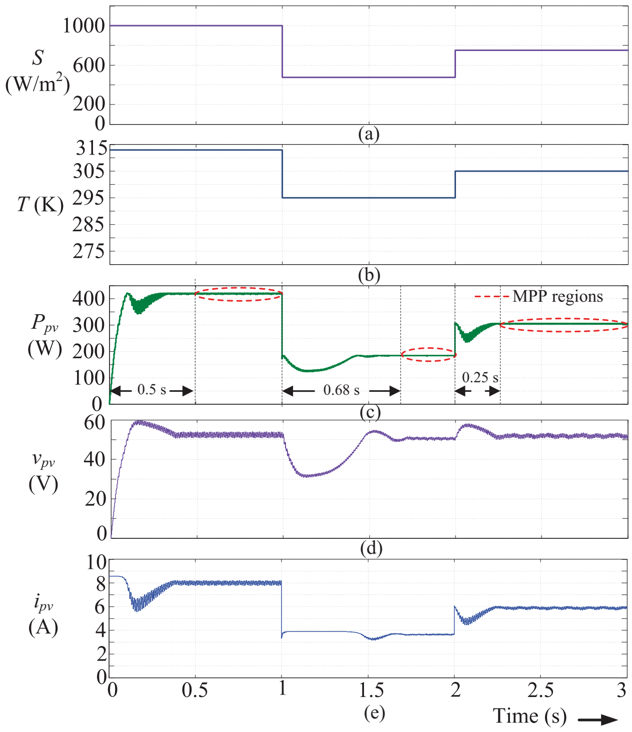

Fig. 10. PV side results. (a) Insolation, (b) Temperature, (c) PV power, (d) PV voltage (V_{pv}) and (e) PV Current (i_{pv}).

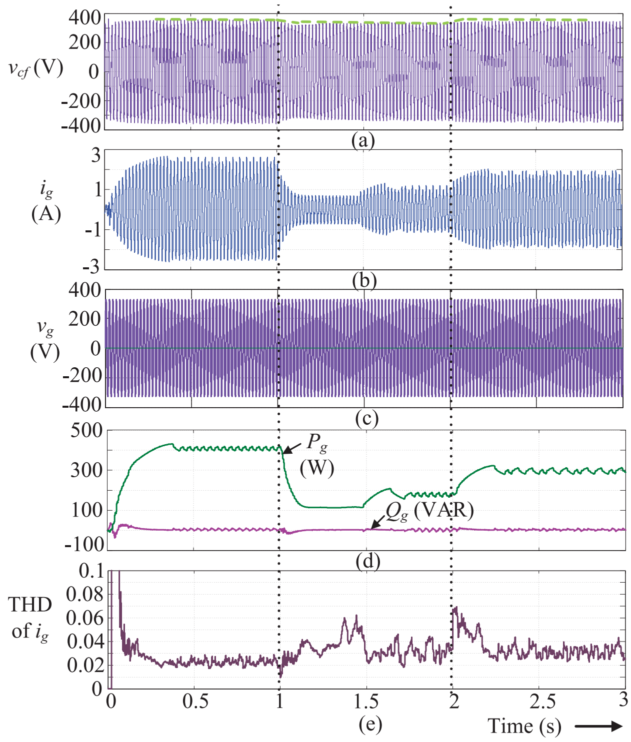

Fig. 11. Grid side results. (a) Capacitor voltage (v_{Cf}), (b) Current pumping into grid (i_g) (c) Grid voltage (v_g), (d) Active and reactive power delivered to grid $(P_g$ & $Q_g)$ and (e) THD of the Current (i_g).

TABLE II
SIMULATION PARAMETERS

Parameter	Value
Voltage (Vmpp at 1000 W/m^2)	52 V
Current (Impp at 1000 W/m^2)	8.3 A
Grid voltage	230 V(RMS)
Grid voltage frequency	50 Hz
Switching frequency of switch (S_p)	50 kHz
Inductor (L_1)	0.35 mH
Inductor (L_2)	1.4 mH
Coefficient of Coupling	0.95
Output capacitor (C_f)	20 μF
Filter inductance (L_f)	0.5 μH
Input filter capacitor (C_P)	4 mF

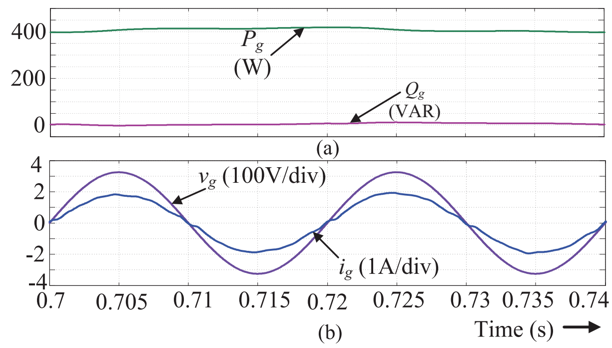

Fig. 12. Zoomed view. (a) Active and reactive power delivered to grid $(P_g$ & $Q_g)$ and (b) Grid voltage (v_g) and Current (i_g).

levels. Obtained grid side results for the tested conditions are shown in Fig. 11. Voltage across C_f (v_{Cf}), grid current (i_g) and grid voltage (v_g) are shown in Fig. 11(a), Fig. 11(b) and Fig. 11(c) respectively. From Fig. 11(a) and Fig. 11(b), it is observed that both (v_{Cf}) and (i_g) are varying according to the tested conditions in order to deliver power at UPF to the grid. From Fig. 11(d), it is confirmed that the system is delivering maximum power obtained from PV to the grid efficiently at UPF. The THD result of grid current (i_g) is shown in Fig. 11(e). The THD value under steady state conditions at each insolation level is observed to be with in 5%. Zoomed view of real and reactive power delivered to the grid are shown in Fig. 12 (a) and zoomed view of grid voltage (v_g) and current pumping into grid (i_g) are shown in Fig. 12(b). From Fig. 12(b), it is clear that both v_g and i_g are in phase with each other confirming the UPF operation. Further, reference reactive power is varied under fixed insolation (at $1000\, W/m^2$) and fixed temperature (323 K), corresponding results are shown in Fig. 13. From $t = 0$ s to $t = 0.9$ s, Q_{ref} is set as 0, at $t = 0.9$ s Q_{ref} is changed to -150 VAR and Q_{ref} is changed to 150 VAR at $t = 1.8$ s. PV power, voltage and current are shown in Fig. 13(a), (b) and (c) respectively. From Fig. 13(a) it is confirmed that the proposed system is tracking constant maximum power under variable reactive power condition. Real and reactive power deliver to the grid are shown in Fig. 13(d). From Fig. 13(d) it is confirmed that the SSCS is tracking the reference reactive power (Q_{ref}) while continuously transferring PV MPP power to grid. Obtained

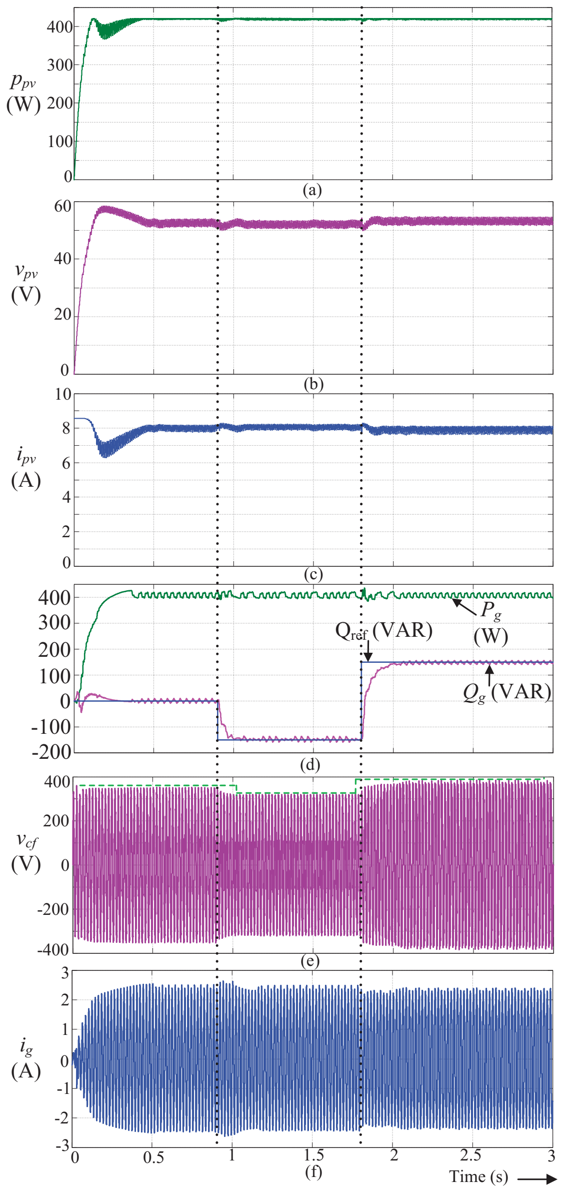

Fig. 13. Reactive power control waveforms. (a) PV power (p_{pv}), (b) PV voltage (v_{pv}), (c) PV current (i_{pv}), (d) Active and reactive power delivered to the grid (p_g & q_g), (e) Voltage (v_{Cf}) and (f) Current (i_g).

voltage (v_{Cf}) and current (i_g) are shown in Fig. 13(e) and (f). v_{cf} in Fig. 13(e) shows that v_{cf} is adjusted in magnitude (can be observed with the dotted line in v_{cf} plot) every time when Q_{ref} is changed such that required amount of active and reactive power are delivered to grid.

V. Conclusion

In this paper a single stage conversion system with reactive power control for PV applications is presented. Control scheme along with derivation of controllers is presented. From the analysis, it can be observed that, system has less switching loss (only one switch operates at high frequency) and is more compact (no additional capacitors are required to trap leakage energy). The system is tested for effective operation under various insolation and temperature conditions and obtained results are satisfactory. Proposed system is tested for different reactive power conditions and results are shown. From the results, it can be concluded that the presented system can effectively control reactive power while tracking MPP.

Acknowledgements

This work is supported by ABB Global Industries and Services Limited, INDIA, under research support program at IIT Madras.

References

[1] D. Meneses, F. Blaabjerg, O. Garcia, and J. Cobos, "Review and Comparison of Step-Up Transformerless Topologies for Photovoltaic AC-Module Application," *IEEE Trans. Power Electron.*, vol. 28, no. 6, pp. 2649–2663, June 2013.

[2] Y. Zhou and W. Huang, "Single-Stage Boost Inverter With Coupled Inductor," *IEEE Trans. Power Electron.*, vol. 27, no. 4, pp. 1885–1893, April 2012.

[3] R. Caceres and I. Barbi, "A boost DC-AC converter: analysis, design, and experimentation," *IEEE Trans. Power Electron.*, vol. 14, no. 1, pp. 134–141, Jan 1999.

[4] S. Jain and V. Agarwal, "A Single-Stage Grid Connected Inverter Topology for Solar PV Systems With Maximum Power Point Tracking," *IEEE Trans. Power Electron.*, vol. 22, no. 5, pp. 1928–1940, Sept 2007.

[5] H. Patel and V. Agarwal, "A Single-Stage Single-Phase Transformer-Less Doubly Grounded Grid-Connected PV Interface," *IEEE Trans. Energy Conv.*, vol. 24, no. 1, pp. 93–101, March 2009.

[6] J. Yris, H. Calleja, L. Hernandez, and J. Olmos, "Design and analysis of a grid-connected inverter without isolation for an AC module," in *Proc. of IEEE Applied Power Electron. and Expo. conf.*, 2012, pp. 2095–2099.

[7] T. Sreekanth, N. L. Narasamma, and Mahesh K. Mishra, "A single stage high gain buck-boost inverter with coupled inductor," in *proc. of IEEE Power Electronics, Drives and Energy Systems Conf.*, 2014, pp. 1–5.

[8] W. Libo, Z. Zhengming, and L. Jianzheng, "A single-stage three-phase grid-connected photovoltaic system with modified mppt method and reactive power compensation," *IEEE Trans. Energy Conv.*, vol. 22, no. 4, pp. 881–886, Dec 2007.

[9] S. H. Hosseini, S. Danyali, and A. Y. Goharrizi, "Single stage single phase series-grid connected pv system for voltage compensation and power supply," in *2009 IEEE Power Energy Society General Meeting*, July 2009, pp. 1–7.

[10] M. Jang, M. Ciobotaru, and V. Agelidis, "A Single-Phase Grid-Connected Fuel Cell System Based on a Boost-Inverter," *IEEE Trans. Power. Electron.*, vol. 28, no. 1, pp. 279–288, Jan 2013.

[11] B. N. Alajmi, K. H. Ahmed, G. P. Adam, and B. W. Williams, "Single-Phase Single-Stage Transformer less Grid-Connected PV System," *IEEE Trans. Power Electron.*, vol. 28, no. 6, pp. 2664–2676, June 2013.

[12] T. Sreekanth, N. L. Narasamma, Mahesh K. Mishra, and S. Augustine, "A single stage coupled inductor based high gain DC-AC buck-boost inverter for photovoltaic (PV) applications," in *Photovoltaic Specialist Conf. (PVSC), 2015 IEEE 42nd*, June 2015, pp. 1–5.

[13] B. Bose, P. Szczesny, and R. L. Steigerwald, "Microcomputer Control of a Residential Photovoltaic Power Conditioning System," *IEEE Trans. Ind. Applications*, vol. IA-21, no. 5, pp. 1182–1191, Sept 1985.

[14] E. G. P. Sanchis, A. Ursaea and L. Marroyo, "Boost dc-ac inverter: a new control strategy," *IEEE Trans. Power Electron.*, vol. 20, no. 2, pp. 343–353, Sept 2005.